Transition Metal B-Site Substitutions in LaAlO3 Perovskites Reorient Bio-Ethanol Conversion Reactions

Quang Nguyen Tran, Olinda Gimello, Nathalie Tanchoux, Monica Ceretti, Stefania Albonetti, Werner Paulus, Barbara Bonelli, Francesco Di Renzo

catalysts

MDPI

Article

Transition Metal B-Site Substitutions in $LaAlO_3$ Perovskites Reorient Bio-Ethanol Conversion Reactions

Quang Nguyen Tran [1,2], Olinda Gimello [1], Nathalie Tanchoux [1], Monica Ceretti [1], Stefania Albonetti [3], Werner Paulus [1], Barbara Bonelli [2] and Francesco Di Renzo [1,*]

1 ICGM, University Montpellier, CNRS, ENSCM, 240 Avenue Emile Jeanbrau, 34296 Montpellier, France; quangnguyenvnp@gmail.com (Q.N.T.); olinda.gimello@enscm.fr (O.G.); nathalie.tanchoux@enscm.fr (N.T.); monica.ceretti@umontpellier.fr (M.C.); werner.paulus@umontpellier.fr (W.P.)
2 DISAT and INSTM Unit of Torino-Politecnico, Politecnico di Torino, Corso Duca degli Abruzzi 24, 10129 Torino, Italy; barbara.bonelli@polito.it
3 Department of Industrial Chemistry Toso Montanari, Alma Mater Studiorum Università di Bologna, Viale Risorgimento 4, 40136 Bologna, Italy; stefania.albonetti@unibo.it
* Correspondence: direnzo@enscm.fr; Tel.: +33-607508148

Abstract: $LaAlO_3$ perovskites, as such and with 25% molar Al substitution by Cu, Co, or Ga, have been prepared by sol-gel methods and tested as heterogeneous catalysts in the gas-phase conversion of ethanol. $LaAlO_3$ presented a significant acidic character, with high formation of ethylene by ethanol dehydration. B-site substitutions increased the basicity of the catalysts, favoring the dehydrogenation of ethanol to acetaldehyde. The most reducible Cu- and Co-substituted materials, characterized by easier formation of surface oxygen vacancies, promoted the self-condensation of acetaldehyde by the Tishchenko mechanism, with formation of acetone and odd-carbon number products. Aldol coupling of acetaldehyde, favored on pure and Ga-substituted $LaAlO_3$, led to the formation of butadiene and hexadiene. The role of Ga insertion, favoring both dehydrogenation of ethylene and dehydration of higher alcohols, corresponds to an amphoteric character. The formation of olefins and diolefins on all catalysts suggests that LaAl-based materials present the most acidic character among La-perovskites.

Keywords: catalysis; oxides; lanthanum; gallium; alcohol reactivity; acetaldehyde; Tishchenko coupling; ethyl acetate; acetone; hydrodeoxygenation

Citation: Tran, Q.N.; Gimello, O.; Tanchoux, N.; Ceretti, M.; Albonetti, S.; Paulus, W.; Bonelli, B.; Di Renzo, F. Transition Metal B-Site Substitutions in $LaAlO_3$ Perovskites Reorient Bio-Ethanol Conversion Reactions. *Catalysts* **2021**, *11*, 344. https://doi.org/10.3390/catal11030344

Academic Editors: Adrian Barroso-Bogeat and Ginesa Blanco

Received: 9 February 2021
Accepted: 1 March 2021
Published: 7 March 2021

1. Introduction

Ethanol is the main chemical commodity issued from renewable resources; more than 90% ethanol being produced by fermentation of biomasses [1]. Bioethanol production of 110 billion liters per year represents more than 70% of the global biofuel market [2]. In the last years, the demand for bioethanol as an additive for automobile fuel has increased rapidly all over the world. Blending bioethanol with conventional fuels is the most easily implementable way to decrease carbon dioxide emission from transportation, as it does not require the introduction of new technologies and can exploit the present fuel supply chain.

Nevertheless, despite proactive blending mandates in more and more countries, the competition of low-cost fossil fuels is a persistent primary barrier which limits the development of biofuels markets [3,4]. Global economic trends related to the Covid-19 pandemics have affected also the biofuel demand, with a drop of 20% in the world bioethanol market and a fall by nearly 50% of the production of bioethanol in the USA [5]. The volatility of biofuel markets concurs with sustainable development issues in fostering alternative outlets to bioethanol production, mainly through the catalytic conversion of ethanol to valuable chemicals or intermediates, reducing the dependence of chemical industry from fossil feedstock. Different catalytic systems guide the ethanol conversion by different routes towards various products [6–9]. Dehydration of ethanol, mainly on acidic catalysts,

forms diethyl ether (a useful solvent) at relatively low temperature and ethylene (the largest produced monomer for polyolefins) at higher temperature [10]. Dehydrogenation of ethanol (usually carried out on supported copper catalysts) forms acetaldehyde, an effective intermediate towards useful monomers, solvents and fuels [11–13]. Ethanol conversion pathways through acetaldehyde lead to the formation of butanol (a performant biofuel) by the Guerbet reaction [14–19] or of butadiene (a major component of elastomers) through the time-honored and recently revamped Ostromislensky and Lebedev processes [20–25]. Successive reactions of acetaldehyde, through coupling with ethanol, aldol coupling and ketonisation, lead to the formation of relevant oxygenated solvents, as ethyl acetate [26,27], acetone [28,29] and 2-pentanone [30]. Propylene (another major monomer for polyolefins) can also be produced from acetaldehyde-derived acetone [31,32].

Steering ethanol reactivity through alternative and successive reaction pathways requires a careful tuning of the acid and base properties of the catalysts. Perovskites are a class of materials in which easily implementable changes of composition allow a precise control of the number and nature of the surface sites [33]. The perovskite structure, with a general formula ABO_3, incorporates both large cations in the cubo-octahedral A site and smaller cations in the octahedral B site [34]. The size of the component ions should abide the Goldschmidt rule, requiring the tolerance factor

$$t = (r_A + r_O)/\sqrt{2(r_B + r_O)} \quad (1)$$

to be in the range from 0.75 to 1, r_A, r_B and r_0 being the ionic radii of the elements in A and B sites and of oxygen. Virtually every large alkaline, alkaline earth, rare earth (or many organic cations) can occupy the site A and the most of smaller transition metal ions are able to occupy the site B. Their different combinations allow about 90% of metallic elements in the periodic table to be crystallized in the perovskite structure [35]. The choice of the component elements allows a fine tuning of the electronic properties [36–38], at the basis of the enormous developments of perovskites in electrode materials, rechargeable batteries, photocatalysis and solar cells [39–45]. In a similar way, oxygen mobility and formation of coordinatively unsaturated sites have been the key properties for the application of perovskites as heterogeneous catalysts [46–49]. La-based perovskites have been proposed as effective catalysts for oxidative steam reforming or mild oxidation reactions [50–52]. Doped La-perovskites can answer environmental concerns for VOC and NOx abatement [53–58], as well as for soot oxidation in diesel exhausts [59,60]. Partial reduction of transition metal components of perovskites has provided interesting, supported catalysts for biomass hydrogenation [61,62].

Steam reforming of ethanol on perovskites has received some attention in the literature, focusing on variously doped $LaNiO_3$ materials [63,64]. Direct conversion of ethanol over perovskite materials in the absence of other reagents was investigated by a limited number of studies, all of which have emphasized the importance of acid-base properties on the catalytic activity. Tesquet et al. investigated the conversion of ethanol over $LaFeO_3$-based catalysts between 300 and 400 °C [65]. They found that basic sites related to the formation of La_2O_3 lead to an increase in the selectivity of butanol and acetone. Chen et al. observed that cation vacancies in nonstoichiometric $LaMnO_3$ catalysts created Lewis acid-base pairs active for the aldolisation of ethanol to form C4 products [66]. Yu et al. suggested that acid-base pairs were formed on $LaMnO_3$ and $LaFeO_3$ by the interaction with a silica support, decreasing the basicity of the stoichiometric perovskites [67]. Un-supported perovskites promoted the formation of acetone, pentanone-2 and ethyl acetate, while supporting on SiO_2 enhanced dehydration reactions and formation of aldolisation products, as 1,3-butadiene and 1-butanol.

The presence of alkaline-earth or rare-earth cations has usually led to stress the activity of perovskites as solid bases, whereas the contribution of acid sites to their surface properties has been more recently highlighted [68]. In this context, the properties of the La-Al_2O_3 materials render the study of LaAl-based perovskites especially relevant. Lan-

thanum impregnation was early suggested as a method to prevent the sintering of γ-Al_2O_3 supports [69]. It was suggested that the surface of the obtained La-Al_2O_3 presented higher acidity than either γ-Al_2O_3 or La_2O_3 [70]. Indeed lanthanum impregnation increased the ethylene selectivity of alumina [71] and the use of La-Al_2O_3 supports increased the acidity of other oxide catalysts [72]. It has been suggested that there is a continuous transition of surface properties between La-Al_2O_3 and $LaAlO_3$ perovskite with the increase of activation temperature, possibly through nonstoichiometric β-Al_2O_3 intermediates [73,74]. The purpose of the present study is to verify the activity of $LaAlO_3$ perovskite in ethanol conversion, a process in which acid-base properties are especially relevant. Partial substitution of Al by other cations, expected to tune the acid-base properties of the materials [75], is an integral part of the study.

2. Results and Discussion

2.1. Characterization of the Catalysts

2.1.1. Phase and Textural Properties

The conversion of ethanol was performed on catalysts denoted as La100, Ga25, Co25, Cu25 on the basis of the fraction of substitution in $LaAlO_3$ perovskite, La100 indicating no substitution and the numbers indicating the percent substitution of Al by any given cation. For instance, Ga25 indicated the composition $LaAl_{0.75}Ga_{0.25}O_3$.

The XRD (X-ray diffraction) pattern of the catalyst, represented in Figure 1, corresponded to single perovskite phases. The cell parameters in the Pm-3m space group are reported in Table 1. Possible rhombohedral distortions could not be reliably measured due to the broad width of the reflections. The cell size of Co25 was analogous to the 3.793 Å one of Al100, in agreement with the similar size of Al^{3+} and Co^{3+} cations, with ionic radii respectively 0.535 and 0.546 Å. Ga25, with the larger Ga^{3+} cation (0.62 Å) and Cu25, with Cu^{2+} (0.69 Å) and the oxygen vacancies induced by the partial replacement of a trivalent by a divalent cation, presented larger 3.816 and 3.811 Å unit cells.

The textural properties of the catalysts determined by N_2 sorption are reported in Table 2 and can be compared with the crystallite size reported in Table 1, as obtained by the Scherrer treatment of XRD line breadth. The specific surface area was in the range 11–16 $m^2\ g^{-1}$, whereas the crystallite size approached 30 nm for all samples. An intergranular mesoporosity between 0.04 and 0.07 $cm^3\ g^{-1}$ was measured, with broad distributions of pore size, centered between 17 and 30 nm, without a well-defined size maximum. Variations in porosity can be attributed to slightly different aggregation of nanocrystals. The N_2 sorption isotherms of the catalysts are reported in Figure S1 in the Supplementary Materials.

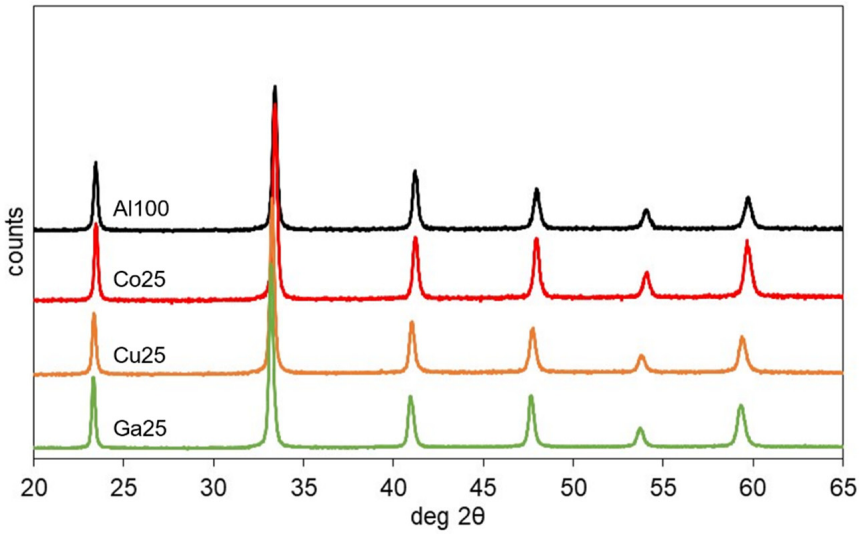

Figure 1. XRD (X-ray diffraction) patterns of the catalysts calcined at 700 °C.

Table 1. Cell parameters and crystallite size of catalysts calcined at 700 °C, after 3 h catalysis test (31% ethanol flow in N_2, 350 °C, weight hour space velocity WHSV 0.23 h^{-1}) and after H_2-TPR (temperature-programmed reduction) experiment. The error in cell parameter is 0.03% and in the crystallite size is 3%.

Catalyst	Cell Size a/Å			$D_{Scherrer}$/nm		
	Calcined at 700 °C	after Catalysis	after H_2-TPR	Calcined at 700 °C	after Catalysis	after H_2-TPR
Al100	3.793	3.794	3.792	30	29	35
Co25	3.794	3.794	3.796	29	29	21
Ga25	3.816	3.815	3.816	29	31	31
Cu25	3.811	3.811	3.805	29	28	30

Table 2. Textural properties of the catalysts. Surface area, pore volume and average pore size as obtained from N_2 sorption isotherms.

Catalyst	S_{BET} m^2 g^{-1}	V_{pore} cm^3 g^{-1}	D_{ave} nm
Al100	14.6	0.07	29
Co25	11.6	0.04	17
Ga25	14.7	0.05	20
Cu25	16.1	0.07	28

2.1.2. Acid-Base Properties

The acid and base characteristics of the catalysts were investigated by isopropanol conversion. The test reaction gives propene and acetone as the main products, as shown in Table 3. The selectivity of conversion depends on the acidity and basicity of the catalysts, the dehydrogenation to acetone being favored on basic sites, whereas the dehydration to propene can occur either on acidic sites or on adjacent acid-base sites [76–78]. For all our catalysts, the main product was acetone, showing a largely basic character. However, the activity and selectivity patterns were not the same on the different catalysts. Ga25 and Co25 presented a nearly complete conversion and a very low selectivity of propene. $LaAlO_3$ had a lower 67% conversion and a 25% selectivity of propene, exhibiting significant acidity alongside a lower activity as basic catalyst.

Table 3. Results of isopropanol conversion tests (4% isopropanol in N_2, 325 °C, WHSV 1.6 h^{-1}).

Catalyst	Conversion %	Carbon Balance %	Selectivity %	
			Acetone	Propylene
Al100	67.8	95.4	74.8	25.2
Co25	98.8	98.7	93.8	6.2
Ga25	97.2	91.5	96.5	3.5

2.1.3. H_2-TPR Experiments

H_2-TPR measurements were performed to investigate the reduction behavior of the catalysts. The hydrogen consumption curves are presented in Figure 2A, unit cell size and Scherrer crystallite size after reduction are reported in Table 1 and the XRD patterns of catalysts after H_2-TPR are shown in Figure S2. Al100 and Ga25 catalysts underwent no measurable reduction in the experimental field. Co- and Cu-substituted samples presented, instead, significant hydrogen consumption (mmol H_2 g^{-1} catalyst).

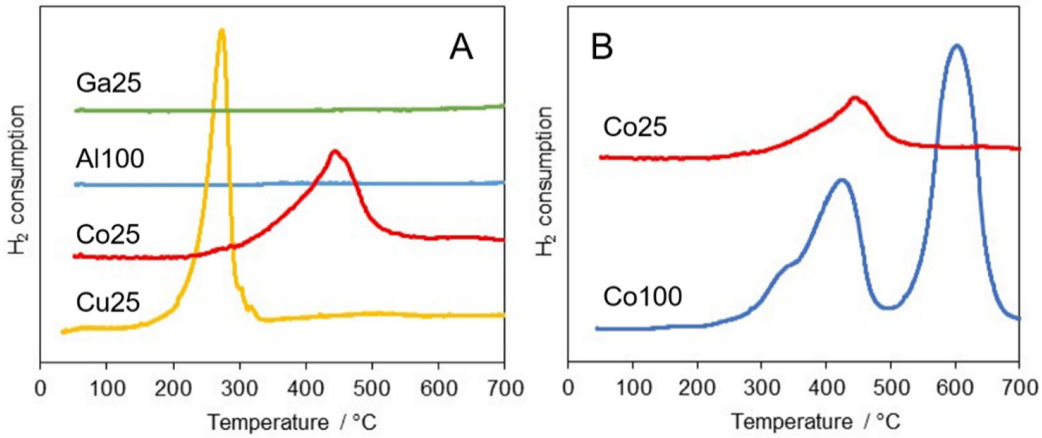

Figure 2. H_2-TPR curves of (**A**) $LaAlO_3$ and B-site substituted catalysts and (**B**) $LaCoO_3$ and mixed La $Al_{0.75}Co_{0.25}O_3$ (Co25). Curves have been shifted for sake of clarity.

Reduction of Cu25 started at nearly 170 °C and featured a sharp peak at 290 °C with consumption of 0.60 mmol g^{-1}. Hydrogen consumption continued in a shallow continuous phenomenon at high temperature, reaching a total of 1.13 mmol H_2 g^{-1}, indicating a total reduction of Cu^{2+} to metallic copper. The amount of hydrogen consumed in the sharp initial peak suggests an intermediate step of reduction of Cu^{2+} to Cu^{+}, followed at higher temperature by a slow reduction of Cu^{+} to Cu^{0} with exsolution of copper from the mixed oxide structure. The XRD pattern after the TPR experiment still presented a well-crystallized perovskite pattern. The shrinkage of the unit cell to values compatible with a defective $LaAlO_3$ phase confirmed the exsolution of copper. Nevertheless, no metallic copper phase was observed, likely due to reoxidation upon exposure of the sample to room atmosphere, with formation of amorphous oxidized copper material.

Co25 TPR showed an asymmetric reduction peak from around 300 to 500 °C, in which 0.40 mmol H_2 per gram of catalyst were consumed, corresponding to the reduction of about 70% Co^{3+} to Co^{2+}. A shallow phenomenon at higher temperature brought the total hydrogen consumption to 0.74 mmol g^{-1}, corresponding to 44% of the hydrogen needed to reduce the cobalt in the sample to metallic cobalt. Ex-situ XRD analysis, carried out after the TPR run, showed that the perovskite structure was preserved, with a significant broadening of the XRD peaks and a swelling of the unit cell, probably related to the inhomogeneous formation of oxygen vacancies [79].

The preservation of the perovskite structure despite significant reduction has to be attributed to the presence of majority Al in the B-site. This effect can be highlighted by comparing the reduction pattern of Co25 with a pure $LaCoO_3$ sample prepared in the same conditions and referred to as Co100 (Figure 2B). The H_2-TPR of Co100 featured two main peaks with maxima at 430 and 600 °C. The total H_2 consumption of 6.1 mmol g^{-1} corresponded to the complete reduction of Co^{3+} to metallic cobalt. Ex-situ XRD pattern after the TPR run indicated a largely amorphous material with no trace of perovskite phase. Only $La(OH)_3$ and minor $La_2O_2CO_3$ phases could be detected, clearly resulting from exposure to room atmosphere of the materials issued from the decomposition of the parent perovskite. In literature reports, it has been shown that Co^{3+} of $LaCoO_3$ can undergo reduction to Co^{0} through a Co^{2+} intermediate with $LaCoO_{2.5}$ brownmillerite structure [80]. This route is referred to as the two-process mechanism, where the hydrogen consumption of the second step ($Co^{2+} + H_2 \rightarrow Co^{0}$) is twice the amount of the first step ($Co^{3+} + 0.5H_2 \rightarrow Co^{2+}$) [81]. In nanocrystalline mixed oxides with higher oxygen mobility, Co^{3+} can be totally reduced also via a one-peak mechanism, in which the two reduction steps are merged [82]. In the case of Co100, the first reduction peak corresponded to the reduction of nearly 45% Co^{3+} to Co^{0}. This result suggests a reduction through mixed two-step and one-step mechanisms, with a relative ratio probably controlled by oxygen diffusion.

2.2. Catalytic Tests

2.2.1. Overview of the Catalytic Activity

The conversion of ethanol followed the main pathways schematized in Figure 3. Ethylene and acetaldehyde were the primary products of dehydration and dehydrogenation reactions, respectively. Further reactions of acetaldehyde can follow different pathways, through aldol coupling or ketonisation reactions. Self-condensation of acetaldehyde to acetaldol (3-hydroxy-butanal) leads to the formation of crotonaldehyde (2-butenal), which is hydrogenated to crotyl alcohol (butenol) or butyraldehyde (butanal), leading to the formation of, respectively, butadiene or longer-chain unsaturated hydrocarbons. Ketonisation of acetaldehyde leads to formation of acetone, which is further converted by transfer hydrogenation and dehydration to propylene or by aldol cross-coupling with acetaldehyde to 2-pentanone and unsaturated C5 hydrocarbons.

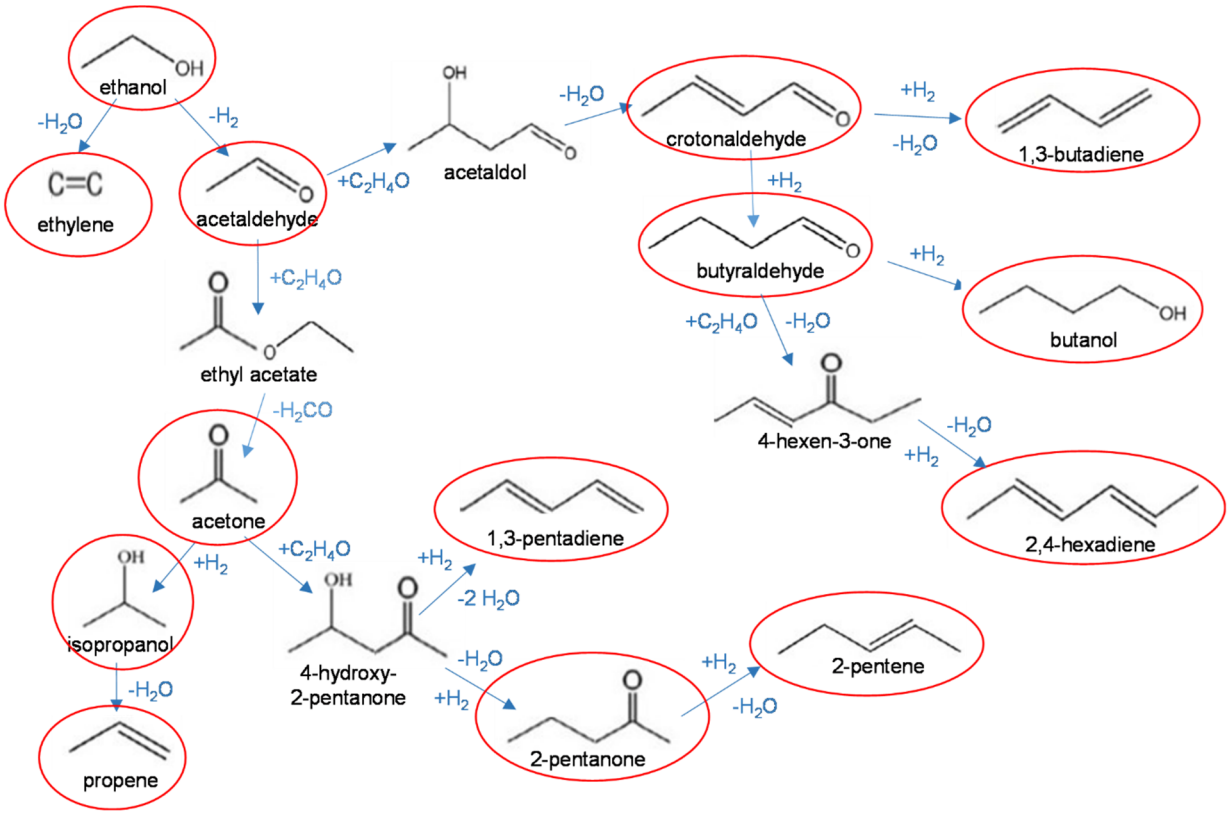

Figure 3. Main reaction pathways in the conversion of ethanol. Products observed in this study are circled in red.

The distribution of products was very different from one catalyst to another, indicating that different reaction pathways were favored. Conversion values and selectivity of the observed products are reported in detail in Table S2 in the Supplementary Information. The selectivity of the most abundant products at 350 °C and 36% conversion are reported in Figure 4. The scale of activity of the catalysts was indicated by the space velocity at which 36% conversion was reached, weight hour space velocity WHSV being 0.011 < 0.020 < 0.023 < 0.028 for, respectively, Cu25, Co25, Al100 and Ga25.

As evidenced in Figure 4, ethylene, the primary dehydration product of ethanol, was the main product for Al100, with a selectivity of 37%. The partial replacement of Al by Cu, Co or Ga brought about a drastic decrease of ethylene yield, the main products being acetaldehyde and acetaldehyde-derived oxygenates. Acetaldehyde was converted to products of consecutive reactions at very different extent according to the nature of the catalyst. On Al100 and Ga25, less than half acetaldehyde was converted to further products. On Cu25 and Co25, nearly 75% acetaldehyde was converted. The main products of acetaldehyde conversion were acetone and 2-pentanone, formed by ketonisation and further

aldol condensation reactions. Acetone further reacted to form 2-pentanone at a different extent according to the type of catalyst. In all cases, the carbon balance was nearly 95%, approaching the maximum possible value. In the evaluation of the carbon balance, it has to be taken into account that the formation of odd-carbon number molecules, like acetone or 2-pentanone, brings about the loss of single-carbon molecules, which were not analyzed. This effect accounts for most of the carbon balance deficit on substituted catalysts.

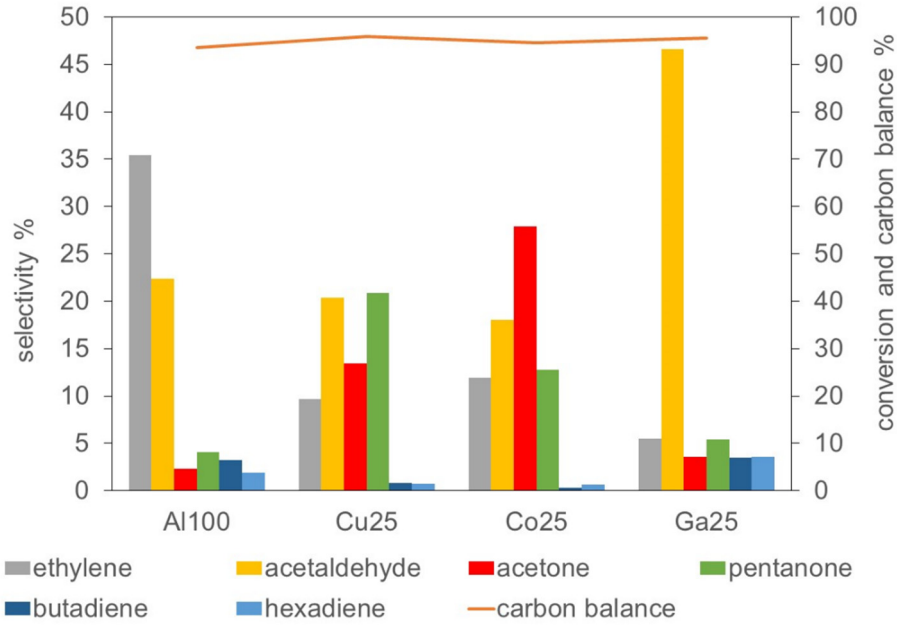

Figure 4. Selectivity and carbon balance of catalytic tests at 350 °C and 36% conversion.

2.2.2. Primary Reactions of Ethanol

The relative activity of the catalysts towards dehydration or dehydrogenation of ethanol can be appreciated by comparing the yield of ethylene (plus minor diethyl ether) with the sum of the yield of acetaldehyde and acetaldehyde-derived products, following the reaction cascades proposed in Figure 3. The yields of dehydration- and dehydrogenation-derived products are reported in Figure 5. In all cases, dehydrogenation prevailed upon dehydration yield, as expected on (mainly basic) lanthanum-containing catalysts. However, the two levels of activity were quite similar on Al100, whereas the substituted catalysts presented a dehydrogenation activity that was by an order of magnitude higher than their dehydration activity. This behavior is in good agreement with the results of the isopropanol test reaction (see Table 3), in which all the catalysts presented a mainly basic behavior but Al100 showed a higher propylene yield, indicating a significant acidic character.

The production of ethylene from ethanol on acid catalysts is a well-known process [10]. Ethylene was clearly produced via dehydration of ethanol over acid catalytic sites, either directly (monomolecular reaction) or through etherification to diethyl ether (bi-molecular path), which was further dehydrated to ethylene. Limited amounts of diethyl ether were observed, with selectivity at 36% conversion up to 1.1% on Al100 and around 0.6% on the substituted catalysts (Table S1). Still lower amount of detected methane and ethane (Table S1) indicated that decomposition and disproportionation reactions did not play a significant role in the reactivity of ethanol [83,84].

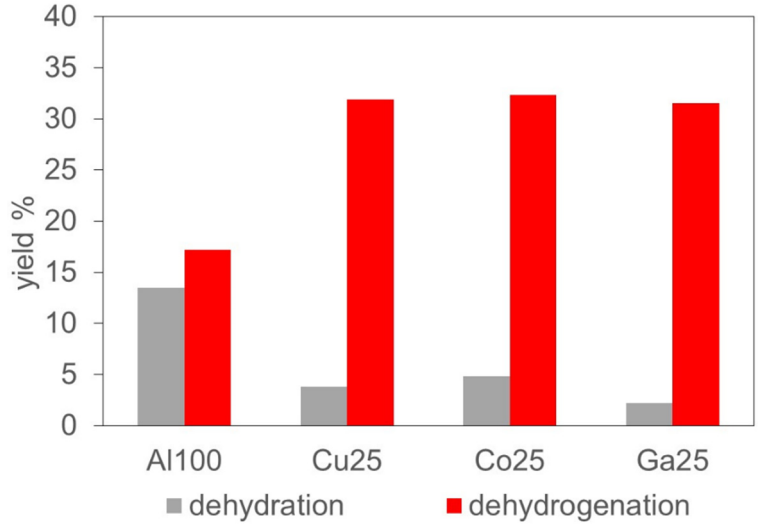

Figure 5. Yield of products issued from different primary reactions of ethanol: dehydration or dehydrogenation. Data at 350 °C, 36% conversion.

2.2.3. Acetaldehyde Reactivity

The conversion of acetaldehyde to further products follows two main pathways: self-condensation to acetaldol or ketonisation to acetone, as schematized as in Figure 3. In order to better compare the reactivity of acetaldehyde on the different catalyst it is interesting to consider the yield of each product on the basis of acetaldehyde rather than of ethanol. The acetaldehyde-based yield can be evaluated as the ratio between the measured amount of a given product and the sum of measured acetaldehyde plus all acetaldehyde-derived products. The fraction of acetaldehyde converted through each step of the reaction cascades is indicated in Figure 6.

Most acetaldehyde was not converted to other products on Ga25 and Al100. The percent fraction of acetaldehyde converted to further products increased in the order 27.1 < 36.7 < 53.6 < 66.8 for, respectively, Ga25, Al100, Cu25 and Co25. In all the cases, more acetaldehyde was converted through the ketonisation pathway than through self-condensation to acetaldol. Other La-based perovskites have indeed been recognized as effective ketonisation catalysts [72]. However, the ratio of conversion between the two pathways was extremely different from one catalyst to another. Conversion through the ketonisation pathway was 1.3 or 1.5 times more effective than the acetaldol pathway in the case of Ga25 or Al100, but was 15 or 20 times more effective for Cu25 or Co25.

Several pathways have been proposed for the ketonisation of acetaldehyde to acetone. The two mainly proposed pathways imply ethyl acetate or acetaldol intermediates. The mechanism of dimerization of acetaldehyde to ethyl acetate, known as the Tishchenko coupling, has been extensively investigated in homogeneous catalysis by Ogata and Kawasaki [85,86] and extended to heterogeneous catalysis by Tanabe and Saito [87].

In the catalytic cycle, an alkoxide complex is formed on a basic site, followed by the nucleophilic attack of the α-carbon by a second acetaldehyde molecule. The formed ethyl acetate species desorbs through hydride exchange with a third acetaldehyde molecule, adsorbed on a Lewis acid site with the regeneration of the alkoxide complex. Formation and desorption of the surface carboxylate have been shown to be favored on bifunctional basic-Lewis acid sites, corresponding to surface oxygen defects easily formed by temperature or redox treatment of basic oxides [88]. This effect has been well documented on $LaCoO_3$ supports [89].

Alternative pathways to ethyl acetate from ethanol have been proposed to take place on the surface of bifunctional Cu-based catalysts. The hemiacetalisation of acetaldehyde with ethanol, followed by a Cu-catalyzed dehydrogenation to ethyl acetate, has been proposed to take place on copper chromite or Cu-Zn-Zr-O catalysts [90,91]. Direct formation of ethyl acetate from ethanol without isolation of an acetaldehyde intermediate has been

proposed to occur on copper chromite by reaction of ethoxide and acylic CH_3CO surface groups formed by dehydrogenation on a copper site [92].

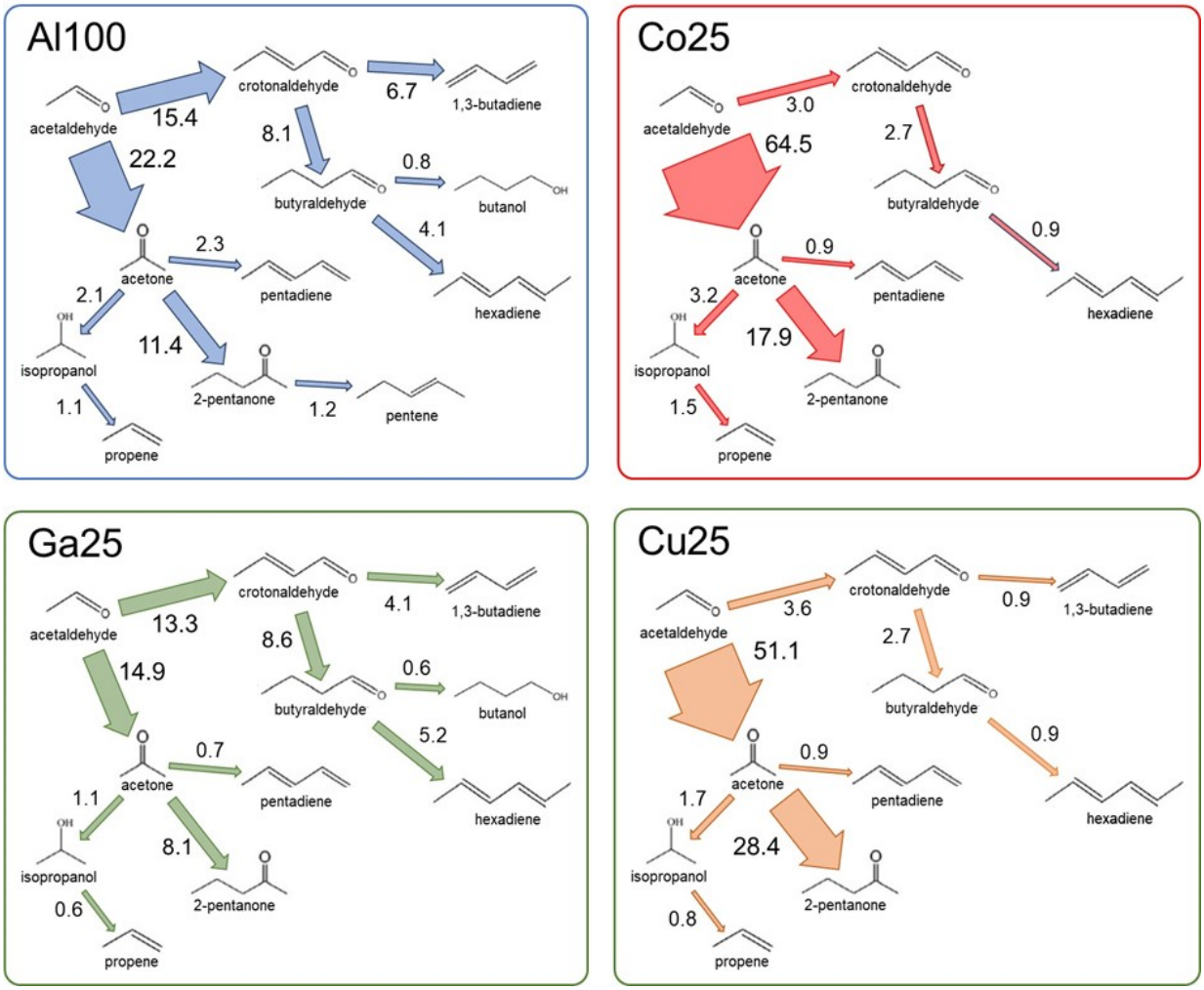

Figure 6. Percent fraction of acetaldehyde converted through each step of different reaction cascades. Data at 350 °C, 36% conversion.

The mechanism of ketonisation of ethyl acetate to acetone has been modelled by Tosoni and Pacchioni on ZrO_2 surface [93]. Ethyl acetate is surface-hydrolysed to acetic acid and ethanol. Ethanol desorbs or contributes as ethoxide to the Tishchenko cycle, whereas adsorbed acetates are converted to enolic CH_2COO^{2-} and acylic CH_3CO surface groups, which condensate to form β-keto butenoic acid, which can easily decarboxylate to form acetone. Oxygen vacancies, deriving from surface reduction, are highly relevant for the critical step of formation of the acetate intermediate.

For all aldehydes with α-hydrogen, like acetaldehyde, the Tishchenko coupling is in competition with the dimerization to acetaldol, usually favored on catalysts with strong basic sites [94]. The formation of acetone through an acetaldol intermediate has been observed on copper catalysts supported on strong basic oxides [95]. In this case, acetone is formed by reverse aldol condensation of the keto form of acetaldol, with evolution of formaldehyde.

In order to assess if the Tishchenko coupling was a suitable pathway to the formation of acetone on our catalysts, ethyl acetate was fed to the reactor in the conditions of the ethanol conversion tests. Conversion and selectivity data are reported in Table 4. Ethyl acetate conversion increased from 20% to 37% in the order Al < Co < Ga. In the meantime, the carbon balance decreased from 97% to 94%. Ethanol, acetone and acetalde-

hyde were the main products formed. The ratio of products was compatible with the ketonisation mechanism of ethyl acetate proposed by Tosoni and Pacchioni [93], through the hydrolytic cleavage of the ester bond at the surface of the catalyst, leading to ethanol release and formation of the surface acetate groups from which acetone is formed. Part of the formed ethanol was dehydrogenated to acetaldehyde, which reacted with acetone to form 2-pentanone. Isopropanol was formed by hydrogenation and dehydration of acetone. Ethylene was formed by thermal decomposition of ethyl acetate [31,96], with an expected parallel formation of acetic acid, which contributed to the surface acetate pool.

Table 4. Results of catalytic conversion of ethyl acetate (1% ethyl acetate in N_2 flow; 350 °C, WHSV 0.19 h^{-1}, 1 h).

Catalyst	Al100	Co25	Ga25
conversion %	19.9	21.0	37.1
C balance %	97.1	96.1	94.4
		selectivity	
ethylene	1.4	0.9	1.7
acetaldehyde	5.0	8.2	11.7
ethanol	44.0	42.0	36.1
acetone	25.7	27.9	23.8
isopropanol	0.2	0.2	1.1
pentanone	0.2	0.7	3.7

2.2.4. Acetone Reactions

Acetone was largely converted by consecutive reactions to other products, the most abundant being 2-pentanone, formed by aldol condensation of acetaldehyde and acetone to 4-hydroxy-2-pentanone and by further hydrodeoxygenation (HDO) to 2-pentanone. More than half acetone was converted to 2-pentanone on Al100, Cu25 and Ga25 catalysts (see Figure 6). On Co25, instead, less than one third of acetone was converted to 2-pentanone, suggesting a lower activity of cross-condensation of acetone and acetaldehyde.

The formation of propene from ethanol by the sequence of reactions: ethanol → acetaldehyde → acetone → propanol → propene was well documented on promoted rare-earth oxides [97,98]. Mixed catalysts formed by basic oxides and acidic zeolites or zirconia were highly effective for this reaction cascade [32,99]. Bifunctional catalysts were indeed needed, as basic functions allowed the dehydrogenation of ethanol to acetaldehyde, paired acid-base sites were needed for the formation of acetone and its transfer hydrogenation to isopropanol, which was dehydrated to propene on acid sites. Among our catalysts, Al100 was significantly more active than the substituted catalysts in several hydrogenation and dehydration reactions of acetone, leading to the formation of propene, as well as of isopropanol, pentene and pentadiene.

2.2.5. Diolefins Formation by Self-Condensation of Acetaldehyde

The self-condensation of acetaldehyde to acetaldol is at the basis of an industrially relevant route of synthesis of long-chain alcohols and diolefins from ethanol [7,8,22]. In the formation of butadiene, acetaldol is dehydrated to form crotonaldehyde (2-butenal), which undergoes a Meerwein-Ponndorf-Verley (MPV) transfer hydrogenation by ethanol to form crotyl alcohol (2-butenol), which is dehydrated to 1,3-butadiene. Among the intermediates in this pathway, acetaldol and butenol were too fast reacting to be observed. Moreover, crotonaldehyde was never observed at selectivity higher than 0.4% (Table S1), confirming its status as a fast-reacting precursor.

Hydrogen from the dehydrogenation of ethanol to acetaldehyde is available in the system and allows the alternative pathway of hydrogenation of crotonaldehyde to butyraldehyde (butanal). Consecutive reactions of butyraldehyde includes MPV hydrogenation to butanol and aldol condensation with acetaldehyde, leading by further dehydration and HDO to the formation of hexadienes. The hydrogenation of crotonaldehyde to bu-

tyraldehyde was always more effective than the HDO to butadiene but the ratio between the two pathways significantly varied among the catalysts. The ratio between formation of butadiene and butyraldehyde was 0.8 > 0.5 > 0.3 > 0.1, respectively on Al100, Ga25, Cu25 and Co25. 2,4-hexadiene was the main products issued from butyraldehyde, through condensation with acetaldehyde and further dehydration and HDO. Butanol was formed only in minor amounts, accounting for no more than 10% of butyraldehyde conversion. It is worth noting that alternative reaction pathways have been proposed for the formation of butanol from ethanol, notably implying a direct self-condensation of ethanol.

2.2.6. Correlations between Activity and Composition of the Catalysts

The formation of significant amounts of C3+ olefins and diolefins differentiates the $LaAlO_3$-based catalysts of this study from other perovskite materials. Perovskites, beyond their activity in redox catalysis, have generally been considered as mainly basic catalysts, leading to the formation of oxygenates. The conversion of ethanol on $LaFeO_3$- or $LaMnO_3$-based perovskites produced oxidized C4 products not observed on $LaAlO_3$-based catalysts in the present study [65–67]. The formation of some butadiene was obtained on $LaMnO_3$ only in the presence of supplementary acid sites provided by the addition of silica [66]. The distribution of products on all the catalysts of the present study indicated a significant activity towards alcohol dehydration and formation of unsaturated hydrocarbons, a trend already observed on lanthanum hydroxides and La-doped aluminas [70,100], but not yet evidenced on La-based perovskites.

In the $LaAlO_3$-based materials of this study, the substitution of a fraction of aluminum by other cations led to a loss of acidity, witnessed by the isopropanol tests and corresponding to a shift of the primary ethanol reactions towards higher formation of acetaldehyde (Figure 5). If this trend of primary reactivity of ethanol can be essentially attributed to a higher basicity of all substituted catalysts, further reactions of acetaldehyde did not follow the same pattern. Cu25 and Co25 catalysts featured a much higher selectivity towards products from Tishchcenko coupling and ketonisation (Figure 6). It is tempting to attribute this effect to the higher reducibility of these catalysts (Figure 2). Mixed oxide catalysts for the synthesis of acetone or pentanone from acetaldehyde are often pre-reduced in H_2 flow before the reaction [30,95]. This treatment has not been applied in our experiments. Nevertheless, the H_2-TPR results showed Cu25 and Co25 to be highly reducible. Moreover, ethanol is an effective reducing agent for copper and cobalt cations in mixed oxides [101]. The diffraction data on substituted $LaAlO_3$ catalysts showed no significant modifications of phase composition and unit cell size between fresh and used catalysts, indicating that ethanol vapor at 350 °C did not bring to a bulk reduction of the catalyst. However, the formation of surface oxygen defects by partial reduction of Co^{3+} by ethanol vapor is a likely occurrence and oxygen defects are expected in Cu25 due to the partial substitution of Al^{3+} by Cu^{2+}. Oxygen vacancies in ZrO_2 have been suggested by Tosoni and Pacchioni to favour the formation of acetone from ethanol by favoring the adsorption on the catalyst of the acetate intermediates [93]. Supported Co_3O_4 has already been shown to be an effective catalyst of Tishchenko coupling [102]. Redox catalysts can indeed be effective for this reaction, despite the mechanism does not imply a formal redox reaction. Very likely, redox modifications of the catalyst in the reaction medium provide the correct type of oxygen vacancies needed for the critical step of Tishchenko coupling, indicated by Tanabe and Saito as the disproportionation between two adsorbed aldehydes to create active surface alkoxides [87].

Ga25, not as reducible as Co25, featured a very limited formation of Tishchenko coupling products, despite a high selectivity in ethanol dehydrogenation to acetaldehyde. This lead to an accumulation of unreacted acetaldehyde. Aldol coupling to acetaldol was the main pathway of condensation of acetaldehyde on Ga25 and Al100, opening the way to the formation of C4 products. Ga25 was the most active catalyst in the formation of butadiene, butyraldehyde and further condensation products, as hexadiene. Al100 was significantly less selective in C4 products, albeit being significantly more selective than

Cu25 and Co25. The role of gallium deserves a special attention, as its position in the periodic table should impart amphoteric properties to its oxide. Gallia has been shown to be more active in dehydrogenation than in dehydration of ethanol [103]. This result is coherent with the high basicity imparted to $LaAlO_3$ by incorporation of gallium, as indicated by the results of isopropanol conversion on Ga25. However, the high effectiveness of Ga25 in the formation of diolefins requires also a good activity in dehydration of alcohols. This has already been observed in the promotion by Ga doping of the formation of butadiene from ethanol in MgO-SiO_2 catalysts for the Lebedev process [25]. In this case, gallium was reputed to introduce Lewis acid sites along the basic sites of the MgO-SiO_2 catalysts, providing acid-base pairs. The concentration of gallium sites was considered critical, the catalytic results presenting a volcano shape with the amount of gallium. This double-faced role of gallium, as well as its poor performance in Tishchenko coupling, suggests that a fine tuning of the relative strength of acid and basic functions is critical for each reaction.

3. Materials and Methods

3.1. Preparation of Catalysts

$LaAlO_3$ catalyst is denoted as Al100 and substituted catalysts are denoted by the symbol of the Al-replacing element and the percent Al replaced. For instance, $LaAl_{0.75}Ga_{0.25}O_3$ is denoted as Ga25. Catalysts were prepared by a sol–gel method. Citric acid was used as a gel-forming agent. $La(NO_3)_3{\cdot}6H_2O$, $Al(NO_3)_3{\cdot}9H_2O$ and $Co(NO_3)_2{\cdot}6H_2O$ from Sigma-Aldrich (Merck, Darmstadt, Germany), and $Ga(NO_3)_3{\cdot}xH_2O$ from Acros Organics (Thermo Fisher Scientific, Waltham, MA, USA) were used as metal precursors. Before synthesis, $Ga(NO_3)_3{\cdot}xH_2O$ was treated by thermal gravimetric analysis to determine its water content. In the preparation, the stoichiometric amount of nitrate salt was dissolved in deionized water. A suitable amount of citric acid (citric acid/metal = 2 mol/mol) was added to the solution, where the pH was kept at 7.5 $\pm$ 0.5 by dropwise addition of ammonia. The solution was stirred and evaporated at 80 °C until the gel was formed. The gel was then kept at 150 °C for 3 h and calcined at 700 °C for 5 h in air flow (heating rate 5 °C min^{-1}).

3.2. Characterisation of Catalysts

Textural properties were assessed by N_2 adsorption at −196 °C using a Tristar instrument (Micromeritics, Norcross, GA, USA) with improved secondary void. Samples were previously outgassed at 250 °C until stable 10 Pa pressure was kept. The surface area was determined by the BET method and the pore volume was measured as the adsorbed amount at p/p° 0.975. Average pore size was determined by the DFT method.

X-ray powder diffraction patterns were collected on a Bruker D8 Advance diffractometer with Bragg-Brentano θ-θ geometry operated with a Cu Kα source (λ = 0.15418 nm). Data analysis was carried out by Rietveld refinement using FullProf 6.10 (2017) software with Thompson-Cox-Hastings pseudo-Voigt shape function. The average crystallite size was calculated by the Scherrer method.

Temperature programmed reduction (H_2-TPR) was investigated using a TPD/R/O 1100 ThermoQuest instrument with a thermal conductivity detector (TCD). In a typical experiment, a quartz tube reactor was loaded with ca. 50–60 mg sample and heated with heating ramp of 10 °C min^{-1}, under 20 mL min^{-1} of 5% H_2/Ar.

3.3. Catalytic Tests

The ethanol conversion was performed in a fixed bed quartz reactor with an internal diameter of 4 mm and a length of 250 mm under atmospheric pressure. Desired ethanol concentration in N_2 carrier gas was achieved by a Bronkhorst CEM (controlled evaporation and mixing) system and space velocity was controlled by changing flow rate. Before feeding ethanol, 100 mg of catalyst was charged into the reactor mixed with silica glass beads and preheated under nitrogen gas at 450 °C in 1 h, before cooling down to the reaction temperature (350 °C). The catalytic reactions were carried out for 6 h on a stream with 1% ethanol in N_2. Tests were carried out with weight space velocities in the range

from 0.1 to 1 $g_{ethanol}$ $g^{-1}{}_{catalyst}$ h^{-1}. The downstream flow was channeled at 150 °C to prevent condensation and was analyzed online by GC Varian 3800 equipped with a Super Q-Plot (30 m length × 0.32 mm id) column and an FID (flame-ionisation detector). Nearly three hours were needed to reach steady state activity. Catalysts were regenerated in air flow at 500 °C. Blank tests were carried out in the absence of catalyst with WHSV 0.23 h^{-1} at 350 °C for 3 h with conversion of 3.5% and acetaldehyde selectivity of 98.5%.

Acid-base properties of catalysts were evaluated in the same experimental system by a model reaction of isopropanol conversion. 4% isopropanol in N_2 was flown through the catalysts at 325 °C at WHSV 1.6 h^{-1} for 90 min. The same reaction system was also used for mechanistic tests in which a possible reaction intermediates, ethyl acetate, was fed to the catalysts at 1% concentration in N_2 at 350 °C at WHSV 0.17 h^{-1} for 3 h.

4. Conclusions

The anoxic conversion of bioethanol, beyond its interest for a sustainable industrial chemistry based on renewable resources, is an excellent test-bed for the evaluation of bifunctional acid-base catalysts. In the case of LaAl-based perovskites, B-site partial substitution of Al significantly affects the catalytic activity, orienting the reactivity towards products as different as polyolefins or oxygenated solvents. $LaAlO_3$-based materials, albeit sharing the main basic character of all lanthanum-based perovskites, present a significant activity in acid-catalyzed reactions. The replacement of a fraction of Al by Cu, Co or Ga decreases increases the basicity of $LaAlO_3$ and favors products formed on bifunctional acid-base sites. The incorporation of easily reducible elements, like Co or Cu, highly increases and modifies the reactivity of the acetaldehyde formed by primary dehydrogenation of ethanol. Tishchenko coupling of acetaldehyde is strongly favored at the expenses of aldol coupling, increasing the ketonisation reaction and the formation of odd carbon-number products. This effect can be accounted for by the formation of Lewis acid-base pairs in correspondence of oxygen defects induced by surface reduction. Deeper characterization of acid-base pairs is a promising field for a better control of the reactivity of acetaldehyde and improve important industrial processes.

Supplementary Materials: The following are available online at https://www.mdpi.com/2073-4344/11/3/344/s1, Figure S1: N_2 sorption isotherms of the catalysts, Figure S2: XRD patterns of catalysts after H_2-TPR. Table S1: Products formed by ethanol conversion at 350 °C, 36 and 60% conversion.

Author Contributions: Conceptualization, F.D.R., Q.N.T. and W.P.; methodology, M.C. and O.G.; investigation, Q.N.T.; resources, S.A., B.B. and N.T.; data curation, F.D.R. and Q.N.T.; writing-original draft preparation, Q.N.T.; writing-review and editing, S.A., B.B. and F.D.R.; supervision, B.B., F.D.R. and W.P. All authors have read and agreed to the published version of the manuscript.

Funding: This work was funded by the SINCHEM Joint Doctorate programme selected under the Erasmus Mundus Action 1 Programme (FPA 2013-0037).

Data Availability Statement: Data is contained within the article and Supplementary Material.

Conflicts of Interest: The authors declare no conflict of interest.

References

1. Ethanol. Available online: https://www.essentialchemicalindustry.org/chemicals/ethanol.html (accessed on 19 September 2020).
2. IEA. Renewables 2019. Available online: https://webstore.iea.org/download/direct/2854?fileName=Renewables_2019.pdf (accessed on 29 January 2021).
3. Lemos, P.; Mesquita, F. Future of Global Bioethanol: An Appraisal of Results, Risk and Uncertainties. In *Global Bioethanol*; Elsevier BV: Amsterdam, The Netherlands, 2016; pp. 221–237.
4. Compare and Contrast Transport Biofuels Policies. Available online: https://www.ieabioenergy.com/wp-content/uploads/2020/03/IEA-Bioenergy-Task-39-Implementation-Agendas-Final-Draft-Feb-4-2020.pdf (accessed on 29 January 2021).
5. Available online: https://www.world-grain.com/articles/13635-global-ethanol-production-could-drop-to-2013-levels (accessed on 22 January 2021).

6. Takei, T.; Iguchi, N.; Haruta, M. Synthesis of Acetoaldehyde, Acetic Acid, and Others by the Dehydrogenation and Oxidation of Ethanol. *Catal. Surv. Asia* **2011**, *15*, 80–88. [CrossRef]
7. Angelici, C.; Weckhuysen, B.M.; Bruijnincx, P.C.A. Chemocatalytic Conversion of Ethanol into Butadiene and Other Bulk Chemicals. *ChemSusChem* **2013**, *6*, 1595–1614. [CrossRef]
8. Sun, J.; Wang, Y. Recent Advances in Catalytic Conversion of Ethanol to Chemicals. *ACS Catal.* **2014**, *4*, 1078–1090. [CrossRef]
9. Garbarino, G.; Pampararo, G.; Phung, T.K.; Riani, P.; Busca, G. Heterogeneous Catalysis in (Bio)Ethanol Conversion to Chemicals and Fuels: Thermodynamics, Catalysis, Reaction Paths, Mechanisms and Product Selectivities. *Energies* **2020**, *13*, 3587. [CrossRef]
10. Zhang, M.; Yu, Y. Dehydration of Ethanol to Ethylene. *Ind. Eng. Chem. Res.* **2013**, *52*, 9505–9514. [CrossRef]
11. Freitas, I.; Damyanova, S.; Oliveira, D.; Marques, C.; Bueno, J. Effect of Cu Content on the Surface and Catalytic Properties of Cu/ZrO2 Catalyst for Ethanol Dehydrogenation. *J. Mol. Catal. A Chem.* **2014**, *381*, 26–37. [CrossRef]
12. Wang, Q.-N.; Shi, L.; Lu, A.-H. Highly Selective Copper Catalyst Supported on Mesoporous Carbon for the Dehydrogenation of Ethanol to Acetaldehyde. *ChemCatChem* **2015**, *7*, 2846–2852. [CrossRef]
13. Garbarino, G.; Riani, P.; García, M.V.; Finocchio, E.; Escribano, V.S.; Busca, G. A Study of Ethanol Dehydrogenation to Acetaldehyde over Copper/Zinc Aluminate Catalysts. *Catal. Today* **2020**, *354*, 167–175. [CrossRef]
14. Marcu, I.-C.; Tanchoux, N.; Fajula, F.; Tichit, D. Catalytic Conversion of Ethanol into Butanol over M–Mg–Al Mixed Oxide Catalysts (M = Pd, Ag, Mn, Fe, Cu, Sm, Yb) Obtained from LDH Precursors. *Catal. Lett.* **2012**, *143*, 23–30. [CrossRef]
15. Scalbert, J.; Thibault-Starzyk, F.; Jacquot, R.; Morvan, D.; Meunier, F. Ethanol Condensation to Butanol at High Temperatures over a Basic Heterogeneous Catalyst: How Relevant Is Acetaldehyde Self-Aldolization? *J. Catal.* **2014**, *311*, 28–32. [CrossRef]
16. Yusoff, M.N.A.M.; Zulkifli, N.W.M.; Masum, B.M.; Masjuki, H.H. Feasibility of Bioethanol and Biobutanol as Transportation Fuel in Spark-Ignition Engine: A Review. *RSC Adv.* **2015**, *5*, 100184–100211. [CrossRef]
17. Sun, Z.; Vasconcelos, A.C.; Bottari, G.; Stuart, M.C.A.; Bonura, G.; Cannilla, C.; Frusteri, F.; Barta, K. Efficient Catalytic Conversion of Ethanol to 1-Butanol via the Guerbet Reaction over Copper-and Nickel-Doped Porous. *ACS Sustain. Chem. Eng.* **2017**, *5*, 1738–1746. [CrossRef]
18. Mazzoni, R.; Cesari, C.; Zanotti, V.; Lucarelli, C.; Tabanelli, T.; Puzzo, F.; Passarini, F.; Neri, E.; Marani, G.; Prati, R.; et al. Catalytic Biorefining of Ethanol from Wine Waste to Butanol and Higher Alcohols: Modeling the Life Cycle Assessment and Process Design. *ACS Sustain. Chem. Eng.* **2019**, *7*, 224–237. [CrossRef]
19. Benito, P.; Vaccari, A.; Antonetti, C.; Licursi, D.; Schiarioli, N.; Rodriguez-Castellón, E.; Galletti, A.M.R. Tunable Copper-Hydrotalcite Derived Mixed Oxides for Sustainable Ethanol Condensation to N-Butanol in Liquid Phase. *J. Clean. Prod.* **2019**, *209*, 1614–1623. [CrossRef]
20. Jones, M.D.; Keir, C.G.; Di Iulio, C.; Robertson, R.A.M.; Williams, C.V.; Apperley, D.C. Investigations into the Conversion of Ethanol into 1,3-Butadiene. *Catal. Sci. Technol.* **2011**, *1*, 267–272. [CrossRef]
21. Sushkevich, V.L.; Ivanova, I.I.; Ordomsky, V.V.; Taarning, E. Design of a Metal-Promoted Oxide Catalyst for the Selective Synthesis of Butadiene from Ethanol. *ChemSusChem* **2014**, *7*, 2527–2536. [CrossRef]
22. Chieregato, A.; Ochoa, J.V.; Bandinelli, C.; Fornasari, G.; Cavani, F.; Mella, M. On the Chemistry of Ethanol on Basic Oxides: Revising Mechanisms and Intermediates in the Lebedev and Guerbet reactions. *ChemSusChem* **2014**, *8*, 377–388. [CrossRef]
23. Baylon, R.A.; Sun, J.; Wang, Y. Conversion of Ethanol to 1,3-Butadiene Over Na doped Zn Zr O Mixed Metal Oxides. *Catal. Today* **2016**, *259*, 446–452. [CrossRef]
24. Ochoa, J.V.; Bandinelli, C.; Vozniuk, O.; Chieregato, A.; Malmusi, A.; Recchi, C.; Cavani, F. An Analysis of the Chemical, Physical and Reactivity Features of MgO–SiO_2 Catalysts for Butadiene Synthesis with the Lebedev Process. *Green Chem.* **2015**, *18*, 1653–1663. [CrossRef]
25. Ochoa, J.V.; Malmusi, A.; Recchi, C.; Cavani, F. Understanding the Role of Gallium as a Promoter of Magnesium Silicate Catalysts for the Conversion of Ethanol into Butadiene. *ChemCatChem* **2017**, *9*, 2128–2135. [CrossRef]
26. Inui, K.; Kurabayashi, T.; Sato, S. Direct Synthesis of Ethyl Acetate from Ethanol Carried Out under Pressure. *J. Catal.* **2002**, *212*, 207–215. [CrossRef]
27. Santacesaria, E.; Carotenuto, G.; Tesser, R.; Di Serio, M. Ethanol Dehydrogenation to Ethyl Acetate by Using Copper and Copper Chromite Catalysts. *Chem. Eng. J.* **2012**, *179*, 209–220. [CrossRef]
28. Murthy, R.; Patnaik, P.; Sidheswaran, P.; Jayamani, M. Conversion of Ethanol to Acetone over Promoted Iron Oxide Catalysis. *J. Catal.* **1988**, *109*, 298–302. [CrossRef]
29. Rodrigues, C.P.; Zonetti, P.C.; Silva, C.G.; Gaspar, A.B.; Appel, L.G. Chemicals from Ethanol—the Acetone One-Pot Synthesis. *Appl. Catal. A Gen.* **2013**, *458*, 111–118. [CrossRef]
30. He, D.; Ding, Y.; Chen, W.; Lu, Y.; Luo, H. One-Step Synthesis of 2-Pentanone from Ethanol over K-Pd/MnOx-ZrO_2-ZnO catalyst. *J. Mol. Catal. A Chem.* **2005**, *226*, 89–92. [CrossRef]
31. Iwamoto, M. Selective Catalytic Conversion of Bio-Ethanol to Propene: A Review of Catalysts and Reaction Pathways. *Catal. Today* **2015**, *242*, 243–248. [CrossRef]
32. Xue, F.; Miao, C.; Yue, Y.; Hua, W.; Gao, Z. Direct Conversion of Bio-Ethanol to Propylene in High Yield over the Composite of in $2O_3$ and Zeolite Beta. *Green Chem.* **2017**, *19*, 5582–5590. [CrossRef]
33. Polo-Garzon, F.; Yang, S.-Z.; Fung, V.; Foo, G.S.; Bickel, E.E.; Chisholm, M.F.; Jiang, D.-E.; Wu, Z. Controlling Reaction Selectivity through the Surface Termination of Perovskite Catalysts. *Angew. Chem. Int. Ed.* **2017**, *56*, 9820–9824. [CrossRef]
34. Mitchell, R.H. *Perovskites Modern and Ancient*; Almaz Press: Thunder Bay, ON, Canada, 2002.

35. Peña, M.A.; Fierro, J.L.G. Chemical Structures and Performance of Perovskite Oxides. *Chem. Rev.* **2001**, *101*, 1981–2018. [CrossRef]
36. Tilley, R.J.D. *Perovskites Structure-Property Relationships*; Wiley: Chichester, UK, 2016; ISBN 0791118935668.
37. Zheng, Y.-S.; Zhang, M.; Li, Q.; Zhu, Y.-A.; Sui, Z.J.; Chen, D.; Zhou, X.-G. Electronic Origin of Oxygen Transport Behavior in La-Based Perovskites: A Density Functional Theory Study. *J. Phys. Chem. C* **2018**, *123*, 275–290. [CrossRef]
38. Zhu, H.; Zhang, P.; Dai, S. Recent Advances of Lanthanum-Based Perovskite Oxides for Catalysis. *ACS Catal.* **2015**, *5*, 6370–6385. [CrossRef]
39. Tejuca, L.G.; Fierro, J.L.G. *Properties and Applications of Perovskite-Type Oxides*; Taylor and Francis: Boca Raton, FL, USA, 1993; ISBN 0-8247-8786-2.
40. Suntivich, J.; May, K.J.; Gasteiger, H.A.; Goodenough, J.B.; Shao-Horn, Y. A Perovskite Oxide Optimized for Oxygen Evolution Catalysis from Molecular Orbital Principles. *Science* **2011**, *334*, 1383–1385. [CrossRef]
41. Wang, W.; Tadé, M.O.; Shao, Z. Research Progress of Perovskite Materials in Photocatalysis- and Photovoltaics-Related Energy Conversion and Environmental Treatment. *Chem. Soc. Rev.* **2015**, *44*, 5371–5408. [CrossRef]
42. Granger, P.; Parvulescu, V.I.; Kaliaguine, S.; Prellier, W. *Perovskites and Related Mixed Oxides-Concepts and Applications*; Wiley-VCH: Weinheim, Germany, 2016; ISBN 978-3-527-33763-7.
43. Grabowska, E. Selected Perovskite Oxides: Characterization, Preparation and Photocatalytic Properties—A Review. *Appl. Catal. B Environ.* **2016**, *186*, 97–126. [CrossRef]
44. Zhang, G.; Liu, G.; Wang, L.; Irvine, J.T.S. Inorganic Perovskite Photocatalysts for Solar Energy Utilization. *Chem. Soc. Rev.* **2016**, *45*, 5951–5984. [CrossRef]
45. Correa-Baena, J.-P.; Saliba, M.; Buonassisi, T.; Grätzel, M.; Abate, A.; Tress, W.; Hagfeldt, A. Promises and Challenges of Perovskite Solar Cells. *Science* **2017**, *358*, 739–744. [CrossRef]
46. Hwang, J.; Rao, R.R.; Giordano, L.; Katayama, Y.; Yu, Y.; Shao-Horn, Y. Perovskites in Catalysis and Electrocatalysis. *Science* **2017**, *358*, 751–756. [CrossRef]
47. Zhu, J.; Li, H.; Zhong, L.; Xiao, P.; Xu, X.; Yang, X.; Zhao, Z.; Li, J. Perovskite Oxides: Preparation, Characterizations, and Applications in Heterogeneous Catalysis. *ACS Catal.* **2014**, *4*, 2917–2940. [CrossRef]
48. Royer, S.; Duprez, D.; Can, F.; Courtois, X.; Batiot-Dupeyrat, C.; Laassiri, S.; Alamdari, H. Perovskites as Substitutes of Noble Metals for Heterogeneous Catalysis: Dream or Reality. *Chem. Rev.* **2014**, *114*, 10292–10368. [CrossRef]
49. Ezbiri, M.; Allen, K.M.; Gàlvez, M.E.; Michalsky, R.; Steinfeld, A. Design Principles of Perovskites for Thermochemical Oxygen Separation. *ChemSusChem* **2015**, *8*, 1966–1971. [CrossRef]
50. Deng, H.; Lin, L.; Liu, S. Catalysis of Cu-Doped Co-Based Perovskite-Type Oxide in Wet Oxidation of Lignin to Produce Aromatic Aldehydes. *Energy Fuels* **2010**, *24*, 4797–4802. [CrossRef]
51. Zhang, J.; Tan, D.; Meng, Q.; Weng, X.; Wu, Z. Structural Modification of $LaCoO_3$ Perovskite for Oxidation Reactions: The Synergistic Effect of Ca^{2+} and Mg^{2+} Co-Substitution on Phase Formation and Catalytic Performance. *Appl. Catal. B Environ.* **2015**, *172–173*, 18–26. [CrossRef]
52. Nguyen, T.H.; Łamacz, A.; Beaunier, P.; Czajkowska, S.; Domanski, M.; Krztoń, A.; Van Le, T.; Djéga-Mariadassou, G. Partial Oxidation of Methane over Bifunctional Catalyst I. In Situ Formation of Ni_0/La_2O_3 During Temperature Programmed POM Reaction over $LaNiO_3$ Perovskite. *Appl. Catal. B Environ.* **2014**, *152–153*, 360–369. [CrossRef]
53. Irusta, S.; Pina, M.; Menendez, M.; Santamaría, J. Catalytic Combustion of Volatile Organic Compounds over La-Based Perovskites. *J. Catal.* **1998**, *179*, 400–412. [CrossRef]
54. Onrubia-Calvo, J.A.; Pereda-Ayo, B.; De-La-Torre, U.; González-Velasco, J.R. Key Factors in Sr-Doped $LaBO_3$ (B = Co or Mn) Perovskites for NO Oxidation in Efficient Diesel Exhaust Purification. *Appl. Catal. B Environ.* **2017**, *213*, 198–210. [CrossRef]
55. Jabłońska, M.; Palkovits, R. Perovskite-Based Catalysts for the Control of Nitrogen Oxide Emissions from Diesel Engines. *Catal. Sci. Technol.* **2019**, *9*, 2057–2077. [CrossRef]
56. Wu, Y.; Li, D.; Lu, J.; Xie, S.; Dong, L.; Fan, M.; Li, B. $LaMnO_3$-La_2CuO_4 Two-Phase Synergistic System with Broad Active Window in Nox Efficient Reduction. *Mol. Catal.* **2020**, *493*, 111111. [CrossRef]
57. Martinovic, F.; Tran, Q.N.; Deorsola, F.A.; Bensaid, S.; Palkovits, R.; Paulus, W.; Bonelli, B.; Di Renzo, F.; Pirone, R. SO_2 Deactivation Mechanism of NO Oxidation and Regeneration of the $LaCoO_3$ Perovskite. *Catal. Sci. Technol.* **2020**, *10*, 2193–2202. [CrossRef]
58. Truong, T.G.; Rotonnelli, B.; Rieu, M.; Viricelle, J.-P.; Kalaitzidou, I.; Marinha, D.; Burel, L.; Caravaca, A.; Vernoux, P.; Kaper, H. Catalytic and Electrochemical Properties of Ag Infiltrated Perovskite Coatings for Propene Deep Oxidation. *Catalysis* **2020**, *10*, 729. [CrossRef]
59. Russo, N.; Furfori, S.; Fino, D.; Saracco, G.; Specchia, V. Lanthanum Cobaltite Catalysts for Diesel Soot Combustion. *Appl. Catal. B Environ.* **2008**, *83*, 85–95. [CrossRef]
60. Tran, Q.N.; Martinovic, F.; Ceretti, M.; Esposito, S.; Bonelli, B.; Paulus, W.; Di Renzo, F.; Deorsola, F.A.; Bensaid, S.; Pirone, R. Co-Doped LaAlO3 Perovskite Oxide for NOx-Assisted Soot Oxidation. *Appl. Catal. A Gen.* **2020**, *589*, 117304. [CrossRef]
61. Escalona, N.; Aranzaez, W.; Leiva, K.; Martinez, N.; Pecchi, G. NI Nanoparticles Prepared from Ce Substituted $LaNiO_3$ for the Guaiacol Conversion. *Appl. Catal. A Gen.* **2014**, *481*, 1–10. [CrossRef]
62. Chen, M.-Y.; Zada, B.; Fu, Y. Perovskite Type Oxide-Supported Ni Catalysts for the Production of 2,5-Dimethylfuran from Biomass-Derived 5-Hydroxymethylfurfural. *Green Chem.* **2016**, *18*, 3858–3866. [CrossRef]

63. Lin, K.-H.; Wang, C.-B.; Chien, S.-H. Catalytic Performance of Steam Reforming of Ethanol at Low Temperature over LaNiO3 Perovskite. *Int. J. Hydrogen Energy* **2013**, *38*, 3226–3232. [CrossRef]
64. Zhang, Q.; Li, L.; Jiang, B.; Wang, K.; Tang, D.; Dou, B. An Intelligent Oxygen Carrier of La−Sr NiO−for Hydrogen Production by Chemical Looping Reforming of Ethanol. *Int. J. Hydrogen Energy* **2017**, *42*, 17102–17111. [CrossRef]
65. Tesquet, G.; Faye, J.; Hosoglu, F.; Mamede, A.-S.; Dumeignil, F.; Capron, M. Ethanol Reactivity over La_1+x FeO_3+δ Perovskites. *Appl. Catal. A: Gen.* **2016**, *511*, 141–148. [CrossRef]
66. Chen, R.-K.; Yu, T.-F.; Wu, M.-X.; Tzeng, T.-W.; Chung, P.-W.; Lin, Y.-C. The Aldolization Nature of Mn4+-Nonstoichiometric Oxygen Pair Sites of Perovskite-Type $LaMnO_3$ in the Conversion of Ethanol. *ACS Sustain. Chem. Eng.* **2018**, *6*, 11949–11958. [CrossRef]
67. Yu, T.-F.; Chang, C.-W.; Chung, P.-W.; Lin, Y.-C. Unsupported and Silica-Supported Perovskite-Type Lanthanum Manganite and Lanthanum Ferrite in the Conversion of Ethanol. *Fuel Process. Technol.* **2019**, *194*, 106117. [CrossRef]
68. Polo-Garzon, F.; Wu, Z. Acid–Base Catalysis over Perovskites: A Review. *J. Mater. Chem. A* **2018**, *6*, 2877–2894. [CrossRef]
69. Church, J.S.; Cant, N.W.; Trimm, D.L. Stabilisation of Aluminas by Rare Earth and Alkaline Earth Ions. *Appl. Catal. A Gen.* **1993**, *101*, 105–116. [CrossRef]
70. Yamamoto, T.; Hatsui, T.; Matsuyama, T.; Tanaka, T.; Funabiki, T. Structures and Acid−Base Properties of La/Al2O3Role of La Addition to Enhance Thermal Stability of γ-Al_2O_3. *Chem. Mater.* **2003**, *15*, 4830–4840. [CrossRef]
71. Garbarino, G.; Wang, C.; Valsamakis, I.; Chitsazan, S.; Riani, P.; Finocchio, E.; Flytzani-Stephanopoulos, M.; Busca, G. Acido-Basicity of Lanthana/Alumina Catalysts and Their Activity in Ethanol Conversion. *Appl. Catal. B Environ.* **2017**, *200*, 458–468. [CrossRef]
72. Klimkiewicz, R.; Trawczyński, J. Secondary Ketonization of Primary Alcohol over Lamn-Based Mixed Oxides with Perovskite-like Structure. *Appl. Catal. A Gen.* **2009**, *360*, 199–204. [CrossRef]
73. Zou, H.; Ge, X.; Shen, J. Surface Acidity and Basicity of γ-Al_2O_3 Doped with K+ and La3+ and Calcined at Elevated Temperatures. *Thermochim. Acta* **2003**, *397*, 81–86. [CrossRef]
74. Delmastro, A.; Geobaldo, F.; Vallino, M.; Abbattista, F. Solid State Equilibria in the System Al_2O_3-La_2O_3-Cr_2O_3: Reactivity Catalyst/Support. *J. Eur. Ceram. Soc.* **1998**, *18*, 607–611. [CrossRef]
75. Foo, G.S.; Polo-Garzon, F.; Fung, V.; Jiang, D.-E.; Overbury, S.H.; Wu, Z. Acid–Base Reactivity of Perovskite Catalysts Probed via Conversion of 2-Propanol over Titanates and Zirconates. *ACS Catal.* **2017**, *7*, 4423–4434. [CrossRef]
76. Gervasini, A. Acidity and Basicity of Metal Oxide Surfaces II. Determination by Catalytic Decomposition of Isopropanol. *J. Catal.* **1991**, *131*, 190–198. [CrossRef]
77. Aramendía, M.; Borau, V.; Jimenez, C.; Marinas, J.; Porras, A.; Urbano, F. Magnesium Oxides as Basic Catalysts for Organic Processes. *J. Catal.* **1996**, *161*, 829–838. [CrossRef]
78. Hattori, H.; Ono, Y. Catalysts and Catalysis for Acid–Base Reactions. In *Metal Oxides in Heterogeneous Catalysis*; Elsevier BV: Amsterdam, The Netherlands, 2018; pp. 133–209.
79. Enriquez, E.; Chen, A.; Harrell, Z.; Dowden, P.; Koskelo, N.; Roback, J.; Janoschek, M.; Chen, C.; Jia, Q. Oxygen Vacancy-Tuned Physical Properties in Perovskite Thin Films with Multiple B-site Valance States. *Sci. Rep.* **2017**, *7*, 46184. [CrossRef]
80. Sis, L.B.; Wirtz, G.P.; Sorenson, S.C. Structure and Properties of Reduced $LaCoO_3$. *J. Appl. Phys.* **1973**, *44*, 5553–5559. [CrossRef]
81. Yang, X.; Yang, L.; Fan, W.; Lin, H. Effect of Redox Properties of $LaCoO_3$ Perovskite Catalyst on Production of Lactic Acid from Cellulosic Biomass. *Catal. Today* **2016**, *269*, 56–64. [CrossRef]
82. Olusola, O.J.; Sudip, M. Temperature Programme Reduction (TPR) Studies of Cobalt Phases in-Alumina Supported Cobalt Catalysts. *J. Pet. Technol. Altern. Fuels* **2016**, *7*, 1–12. [CrossRef]
83. Dewilde, J.F.; Czopinski, C.J.; Bhan, A. Ethanol Dehydration and Dehydrogenation on γ-Al_2O_3: Mechanism of Acetaldehyde Formation. *ACS Catal.* **2014**, *4*, 4425–4433. [CrossRef]
84. Malmusi, A.; Ochoa, J.V.; Tabanelli, T.; Basile, F.; Lucarelli, C.; Agnoli, S.; Carraro, F.; Granozzi, G.; Cavani, F. Ethanol Aerobic and Anaerobic Oxidation with $FeVO_4$ and V_2O_5 Catalysts. *Appl. Catal. A Gen.* **2019**, *570*, 139–147. [CrossRef]
85. Ogata, Y.; Kawasaki, A.; Kishi, I. Kinetics of the Tischenko Reaction of Acetaldehyde with Aluminium Isopropoxide. *Tetrahedron* **1967**, *23*, 825–830. [CrossRef]
86. Ogata, Y.; Kawasaki, A. Alkoxide Transfer from Aluminium Alkoxide to Aldehyde in the Tishchenko Reaction. *Tetrahedron* **1969**, *25*, 929–935. [CrossRef]
87. Tanabe, K. The Conversion of Benzaldehyde into Benzyl Benzoate with Alkaline Earth Metal Oxide Catalysts. *J. Catal.* **1974**, *35*, 247–255. [CrossRef]
88. Seki, T.; Nakajo, T.; Onaka, M. The Tishchenko Reaction: A Classic and Practical Tool for Ester Synthesis. *Chem. Lett.* **2006**, *35*, 824–829. [CrossRef]
89. Bonne, M.; Bion, N.; Pailloux, F.; Valange, S.; Royer, S.; Tatibouët, J.-M.; Duprez, D. Improved Oxygen Mobility in Nanosized Mixed-Oxide Particles Synthesized Using a Simple Nanocasting Route. *Chem. Commun.* **2008**, 4504–4506. [CrossRef]
90. Zonetti, P.C.; Celnik, J.; Letichevsky, S.; Gaspar, A.B.; Appel, L.G. Chemicals from Ethanol—The Dehydrogenative Route of the Ethyl Acetate One-Pot Synthesis. *J. Mol. Catal. A Chem.* **2011**, *334*, 29–34. [CrossRef]
91. Carotenuto, G.; Tesser, R.; Di Serio, M.; Santacesaria, E. Kinetic Study of Ethanol Dehydrogenation to Ethyl Acetate Promoted by a Copper/Copper-Chromite Based Catalyst. *Catal. Today* **2013**, *203*, 202–210. [CrossRef]

92. Colley, S.W.; Tabatabaei, J.; Waugh, K.C.; Wood, M.A. The Detailed Kinetics and Mechanism of Ethyl Ethanoate Synthesis over a Cu/Cr_2O_3 Catalyst. *J. Catal.* **2005**, *236*, 21–33. [CrossRef]
93. Tosoni, S.; Pacchioni, G. Acetic Acid Ketonization on Tetragonal Zirconia: Role of Surface Reduction. *J. Catal.* **2016**, *344*, 465–473. [CrossRef]
94. Hattori, H. Heterogeneous Basic Catalysis. *Chem. Rev.* **1995**, *95*, 537–558. [CrossRef]
95. Xu, M.; Gines, M.J.; Hilmen, A.-M.; Stephens, B.L.; Iglesia, E. Isobutanol and Methanol Synthesis on Copper Catalysts Supported on Modified Magnesium Oxide. *J. Catal.* **1997**, *171*, 130–147. [CrossRef]
96. Vargas, D.C.; Salazar, S.; Mora, J.R.; Van Geem, K.M.; Streitwieser, D.A. Experimental and Theoretical Study of the Thermal Decomposition of Ethyl Acetate during Fast Pyrolysis. *Chem. Eng. Res. Des.* **2020**, *157*, 153–161. [CrossRef]
97. Mizuno, S.; Kurosawa, M.; Tanaka, M.; Iwamoto, M. One-Path and Selective Conversion of Ethanol to Propene on Scandium-modified Indium Oxide Catalysts. *Chem. Lett.* **2012**, *41*, 892–894. [CrossRef]
98. Hayashi, F.; Iwamoto, M. Yttrium-Modified Ceria as a Highly Durable Catalyst for the Selective Conversion of Ethanol to Propene and Ethene. *ACS Catal.* **2012**, *3*, 14–17. [CrossRef]
99. Matheus, C.R.V.; Chagas, L.H.; Gonzalez, G.G.; Aguiar, E.F.S.; Appel, L.G. Synthesis of Propene from Ethanol: A Mechanistic Study. *ACS Catal.* **2018**, *8*, 7667–7678. [CrossRef]
100. Valsamakis, I.; Garbarino, G. Lanthanum-Based Catalysts for (Bio)Ethanol Conversion: Effect of Preparation Method on Catalytic Performance—Hard Tem-Plating versus Hydrolysis. *J. Chem. Technol. Biotechnol.* **2020**, *6627*, 1–6627. [CrossRef]
101. Vozniuk, O.; Bazzo, C.; Albonetti, S.; Tanchoux, N.; Bosselet, F.; Millet, J.-M.M.; Di Renzo, F.; Cavani, F. Structural Changes of Binary/Ternary Spinel Oxides During Ethanol Anaerobic Decomposition. *ChemCatChem* **2017**, *9*, 2219–2230. [CrossRef]
102. Jagadeesh, R.V.; Junge, H.; Pohl, M.-M.; Radnik, J.; Brückner, A.; Beller, M. Selective Oxidation of Alcohols to Esters Using Heterogeneous Co3O4–NC Catalysts under Mild Conditions. *J. Am. Chem. Soc.* **2013**, *135*, 10776–10782. [CrossRef]
103. Izzo, L.; Tabanelli, T.; Cavani, F.; Vàsquez, P.B.; Lucarelli, C.; Mella, M.; Blair, P. The Competition between Dehydrogenation and Dehydration Reactions for Primary and Secondary Alcohols over Gallia: Unravelling the Effects of Molecular and Electronic Structure via a Two-Pronged Theoretical/Experimental Approach. *Catal. Sci. Technol.* **2020**, *10*, 3433–3449. [CrossRef]